Advanced Steel Construction – Vol. 18 No. 1 (2022) 453–464
DOI:10.18057/IJASC.2022.18.1.4

EXPERIMENTAL, NUMERICAL, AND THEORETICAL STUDY ON STATIC BEHAVIOUR OF NOVEL STEEL DOVETAIL JOINT SUBJECTED TO AXIAL TENSILE LOAD

Waleed Mashrah [1], Zhi-Hua Chen [1, 2, 4], Hong-Bo Liu [3, *] and Mohammed Ameen Amer [1]

[1] *Department of Civil Engineering, Tianjin University, Tianjin 300072, China*
[2] *State Key Laboratory of Hydraulic Engineering Simulation and Safety, Tianjin University, Tianjin 300072, China*
[3] *Department of Civil Engineering, Hebei University of Engineering, Handan 056000, China*
[4] *Key Laboratory of Coast Civil Structure and Safety of Ministry of Education, Tianjin University, Tianjin 300072, China*
** (Corresponding author: E-mail: hbliu@tju.edu.cn)*

ABSTRACT

In this study, two types of socket joints manufactured based on a simple design concept and bearing load principle are proposed. The design concept, design method, test program, and FE modelling method for a novel steel dovetail joint without teeth pattern (Interlock type I) and with teeth pattern (Interlock type II) are also discussed. In addition, the tests and numerical analyses of four specimens were conducted to investigate the bearing capacities and failure modes of the new joint systems under axial tensile loads. The test results indicated that the specimens with and without teeth patterns exhibited different tensile bearing capacities: the specimens with teeth patterns generated twice the tensile load capacity of those without teeth patterns. This result can be attributed to the fact that the interlock type-II specimens rely on the teeth pattern, edges of the hub keyway, and hub ring to bear the load, whereas interlock type-I specimens rely only rely on the edges of the hub keyway and hub rings. Further, the two types of specimens have the same failure modes when the beam-inserted end (tail) is pulled out of the hub keyway. In addition, shear failure occurs on the teeth pattern of the hub keyways and beam-inserted ends of the interlock type-II specimens. Two FE models are established to verify the results of the tests, and the related equations are derived and calculated. The results obtained from the numerical analysis using the equations were compared with the test results. Finally, it was concluded that the results obtained using the three analysis methods adopted in this study agree very well, with high calculation validity and efficiency.

ARTICLE HISTORY

Received: 10 February 2021
Revised: 26 May 2021
Accepted: 26 May 2021

KEYWORDS

New socketed join;
Novel steel dovetail joint;
H-shaped beam;
Tensile bearing capacity;
Failure mode

1. Introduction

In the past two decades, single-layer grid shell structures with complex curved surfaces have been designed for structural application in leisure destinations, transportation, theatres, airports, museums, and so on, demonstrating outstanding architectural and structural representation at reasonable cost [1]. Therefore, the design and optimisation of a joint system for single-layer grid shells has become one of the most active research topics in spatial structures [2]. The grid shells rely on the connection type to transfer loads. Therefore, the mechanical performance of the joint system directly impacts the bearing capacity and safety of the grid shells [3]. The joints used in these structures can be classified into assembled and welded joints [4]. Further, the assembled joints can be categorised as bolted and socketed joints.

Traditional welded joints are widely used in steel structures, particularly in welded hollow spherical joints, which have been in service for more than 54 years [5][6], and tubular joints [7]. However, because of the difficulties and challenges of using welded joint systems, several engineers have proposed a new type of bolted joint system to secure the quick development of steel structures including single-layer grid shells such as bolted joints (Fig. 1), mero joints [8], bolt–ball joints [9], bolted beam-to-column connections [10], double-ribbed reinforced beam–column connections [11], and tremor joints of aluminium (Fig. 2) [12] and a few types of socketed joints such as socket [13][14] and triodetic joints [15].

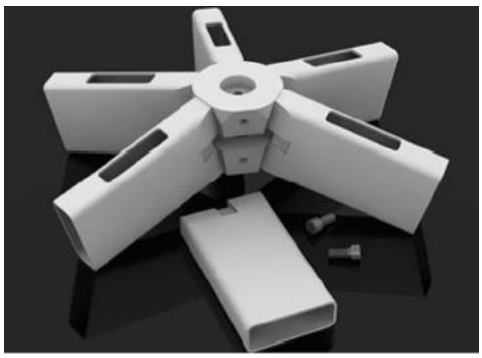

Fig. 1 Bolted joint [1]

Fig. 2 Greenhouse exhibition hall in a botanical garden in Shanghai, China [12]

Recently, numerical and experimental approaches have been employed to investigate the mechanical performance of steel structure joints under various load conditions. Qiao et al. [16] examined the moment–rotation relationship of steel sleeve beam- column joints using interference FITs. Shen Yan et al. [17] carried out a series of tests to study the full-range behaviour of steel beam-to-column connections. Zhe et al. [18] carried out a numerical study based on the test results of previous studies on the behaviour of Temcor joints under bending and axial loads. Han et al. [3][19] conducted experiments to examine the behaviour of assembled joints (AHs) under tension, compression, and bending moments. In their study, the results of the FE and theoretical analyses matched well with the elastic stiffness and bearing capacities of the assembled joint specimens in the tests. Ma et al. [20] performed a series of tests on a gear–bolt joint, considering various design parameters. Oyeniran et al. [21] experimentally and numerically studied the performance of aluminium bolted joints (HBJs) under axial loads. Fan et al. [22] adopted an experimental approach to investigate the moment–rotation relationship for a semirigid joint system connector under various loading schemes. Ma et al. [23] used experimental and numerical approaches to investigate the mechanical performance of new semirigid joints by considering different design parameters. They also adopted the same approaches to investigate the gear–bolt and bolt–column (BC) joint behaviours under a bending moment. In addition, several joints were designed using the various shapes of the sections of members, such as circular tubes, rectangular tubes, and H-shaped members. Ma et al. [4] investigated the static behaviour of bolt–column joints with

rectangular section members under in-plane direction bending. Konstantinos et al. [24] Ma et al. [25], and Han et al. [2][3][19] designed and tested various types of joints with rectangular section members. A joint with a circular section is the most popular one and applicable to single-layer grid shells. Xue et al. [26] performed experimental and numerical analyses to investigate a new type of single-layer reticulated shell connection (TCS) under a bending moment. Liu et al. [5] experimentally and numerically investigated the residual behaviour of welded hollow spherical joints under corrosion and de-rusting. Thus, various connections with circular tube members have been developed and investigated, such as bolt–ball joints with circular steel tubes [27], semirigid joints [22], socket joints [13], and welded hollow spherical joints [28]. In contrast, a few joints are designed using H-section beams; these exclude the Temcor (Figs 3 and 4) [29][30] and welded hollow spherical joints (Fig. 5) [31].

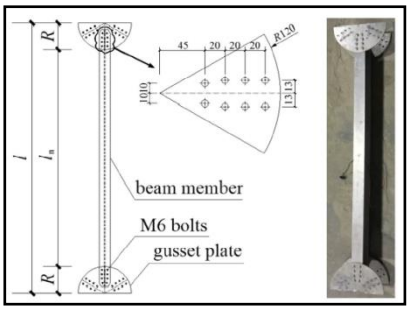

Fig. 3 Beam member of Temcor joint [29]

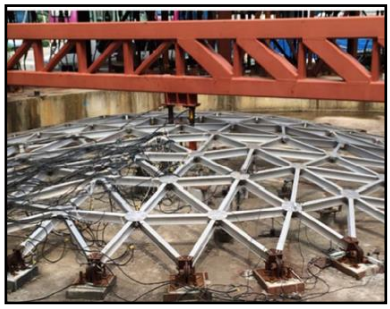

Fig. 4 Temcor joint experimental shell [30]

Fig. 5 Welded hollow spherical joint with H-section beam [31]

H-shaped members present the advantages of reducing the material, weight, and cost of the structure because they have weak and strong axes of inertia moment. However, the only assembled joint that is designed and developed using an H-shaped beam is a Temcor joint. Joints such as Temcor only connect the upper and lower flanges of the H-shaped beam with the upper and lower gusset plates without connecting the H-shaped beam; thus, a weak shear deformation can occur in this type of joint. In this study, a novel steel dovetail joint with the H-shaped beam and socket concept was proposed to avoid the problems encountered using the other types of joints.

2. Concept of novel steel dovetail joint

Two types of novel steel dovetail joints have been designed in this study using H-shaped members, combining the hub and socket concepts. The dovetail mortise–tenon concept is generally used in connections among timber structures, such as those among the ancient Chinese timber structures (Fig. 6) [32][33][34]. In this hub system, the hub or joint plate is placed at the centre of the joint, and the elements connect to the centre as rays, as illustrated in the hub joint of steel and triodetic joint of aluminium (Fig. 7). Novel steel dovetail joints with interlocks type I (NDJs) and type II (NDJGs) are designed based on these two concepts (Fig. 8).

The novel steel dovetail joint contains a hexagonal hub with three removed areas (Figs 9 and 10) to reduce the self-weight of the hub. The second component of this novel steel dovetail joint is an H-shaped beam with four main parts: an H-shaped member with curved flanges, throat web, throat neck, and beam-inserted end (tail). The beam throat is welded to the H-shaped member; thereafter, the beam end is inserted into the hub keyway. The joint is completed when two cover plates with the same shape as that of the extrude hub are arranged at the ends of the hub and a screwed bolt passed through the hub centre to connect the cover plates. Two types of novel steel dovetail joints are designed based on the same concept and specifications; the only difference is the interlock system: the interlock type-I specimens (NDJs) are designed using the standard dovetail shape (Fig. 11), whereas the interlock type-II specimens (NDJGs) are designed with teeth patterns in their interlock system (Fig. 12).

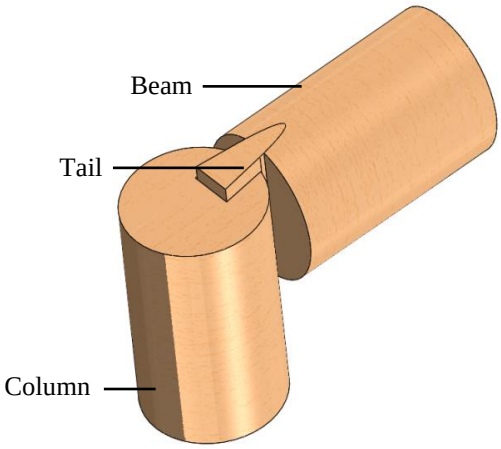

Fig. 6 Mortise–tenon system

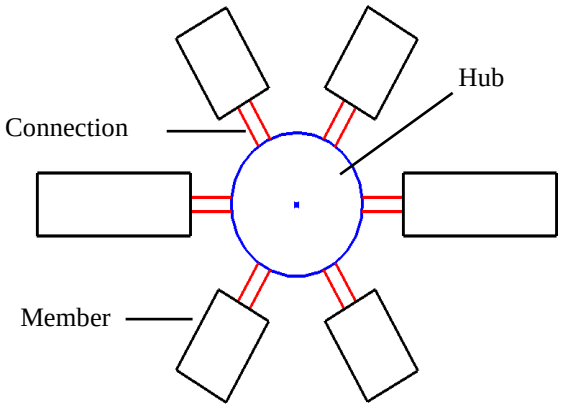

Fig. 7 Hub system

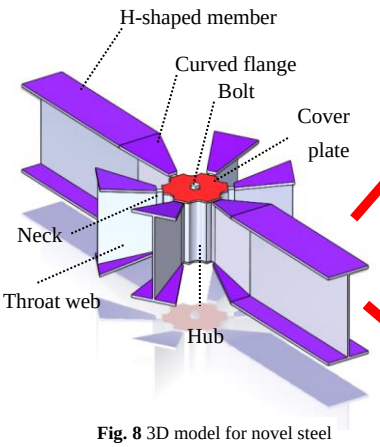

Fig. 8 3D model for novel steel dovetail joint system

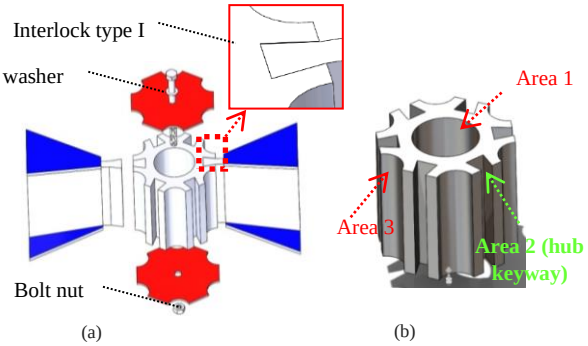

Fig. 9 3D model for novel steel dovetail joint (NDJ type): (a) Interlock type I, (b) hub type I

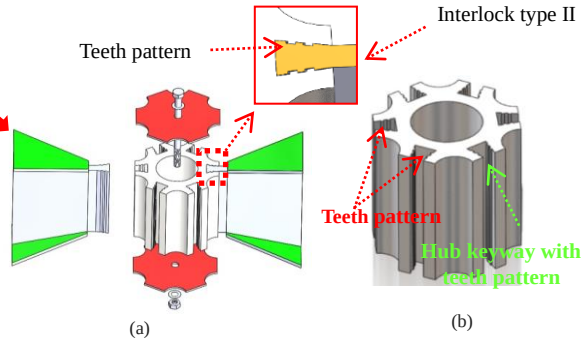

Fig. 10 3D model for novel steel dovetail joint (NDJG type): (a) Interlock type II, (b) hub type II

.

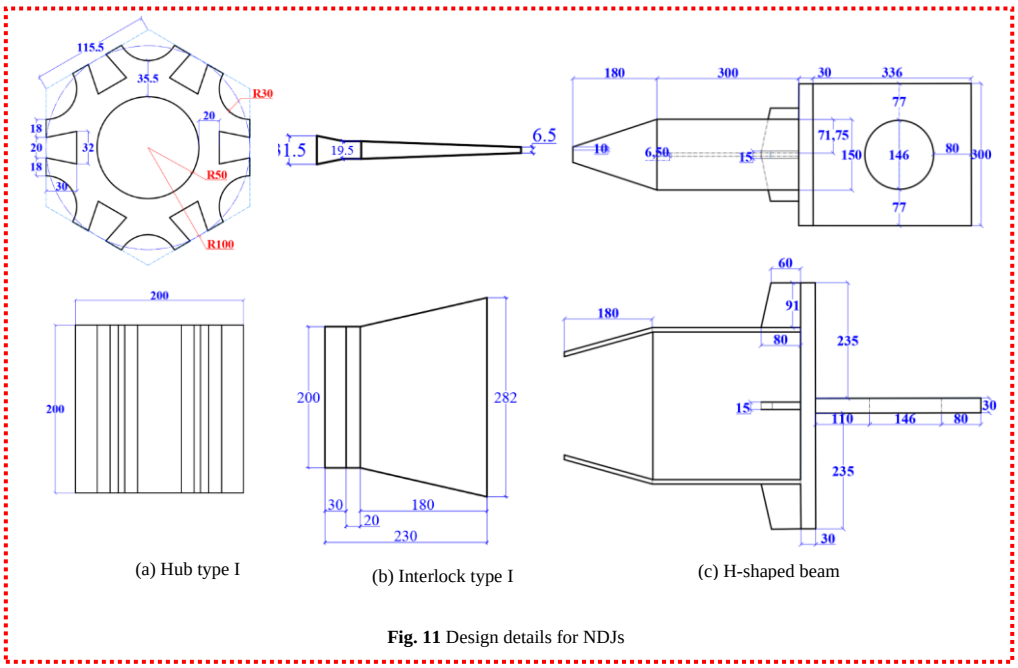

Fig. 11 Design details for NDJs

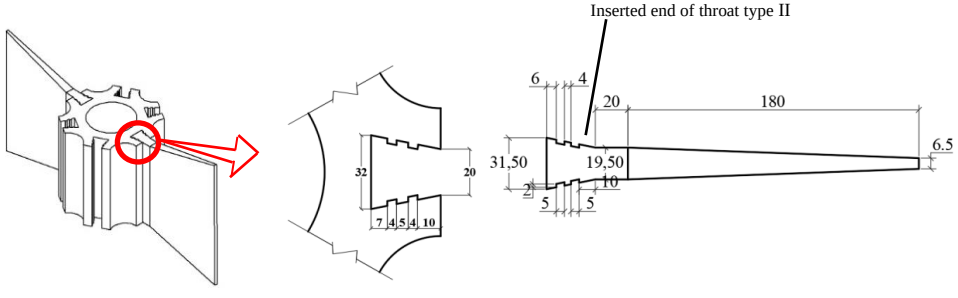

Fig. 12 Design details for NDJGs

3. Test program

3.1. Design of specimens

In this section, the investigation of the mechanical performance and failure modes of the new joint system under axial tensile load is described. Two specimens each of the novel steel dovetail joint with interlock type I (NDJ-1 and NDJ-2) and interlock type II (NDJG-1 and NDJG-2) were designed. The four specimens were assembled after fabrication and transported to the Tianjin University laboratory (Fig. 13 (a) and (b)). Thereafter, NDJG-1 and NDJG-2 were designed using interlock type II with teeth patterns to improve the performance of this new joint system under tensile load. After the specimens were assembled, all the test preparations were completed, and the specimens were placed in the test machine (Fig. 13 (c) and (d)).

Tension loads were applied to the novel steel dovetail joints using a horizontal hydraulic jack with a load capacity of 15000 kN. Therefore, to investigate the tensile bearing capacities and failure modes of these new joints, all the test specimens were designed with a loading plate and circular opening at the centre to fit the connecting elements of the loading machine (Fig. 13 (b) and (d)).

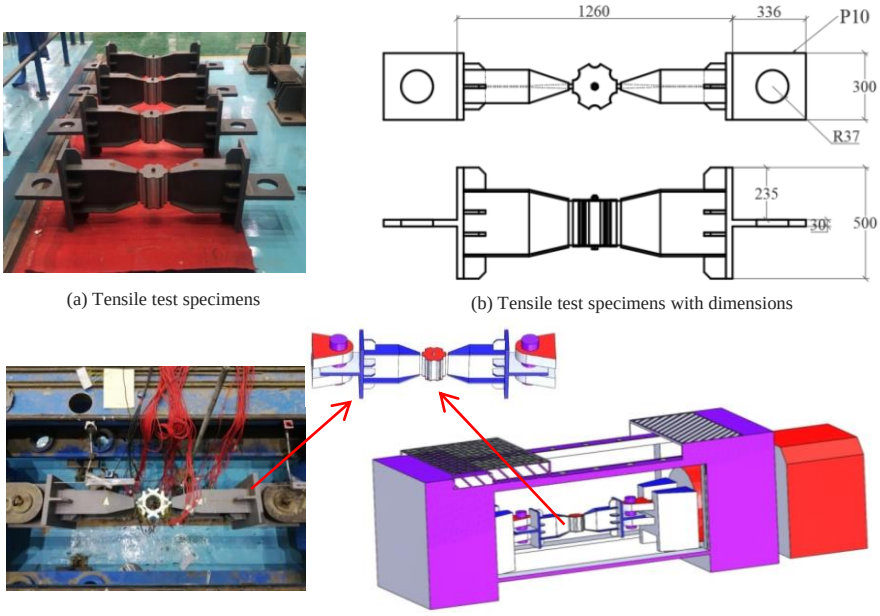

(a) Tensile test specimens

(b) Tensile test specimens with dimensions

(c) Loading the test specimen

(d) Tensile test machine

Fig. 13 Test program for novel steel dovetail joint

3.2. Arrangement of measuring points

The applied load was measured by the load sensor in the loading machine, and four displacement sensors were used to measure the axial deformation of the specimens under axial tension load (DG1 to DG4) (Fig. 14). Simultaneously, to measure the strain, 42 gauges were arranged on the test specimens, as displayed in Fig. 14 (a) and (b). The strain gauges were set mainly on the internal and external faces of the hub ring, beam neck, H-shaped beam web, and curved flanges and around the throat with the beam-welded area.

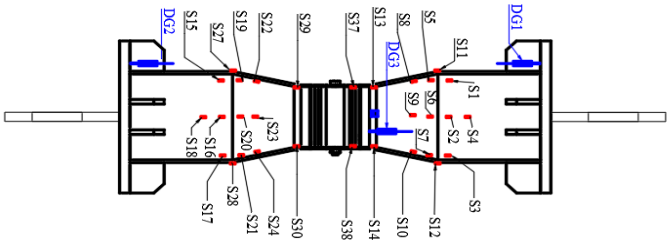

(a) Side view

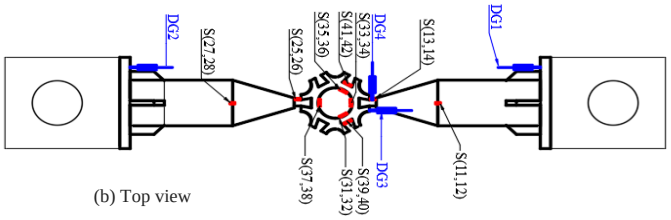

(b) Top view

Fig. 14 Arrangement of measurement points

3.3. Material test

All the components of the novel steel dovetail joint were designed using steel Q345. The material test is one of the most essential tests in structural engineering research. Therefore, to determine the stress–strain behaviour of the materials, a standard material tensile test should be conducted. Four groups of specimens were tested for the hub, throat, H-shaped beam flanges, and H-section beam web (Fig. 15). The material test model parameters and results are presented in Table 1 and Fig. 16. The material shear strength f_v was calculated according to the shear strength of the materials as specified in the Chinese code for the design of steel structures (GB 50017-2003) [35].

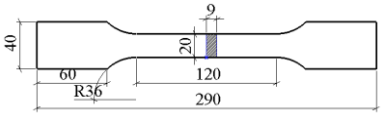

(a) Specimen design for flange

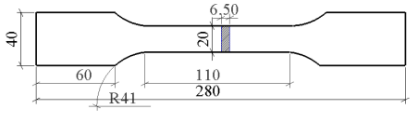

(b) Specimen design for web

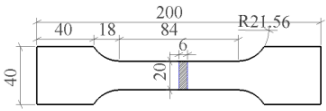

(c) Specimen design for hub

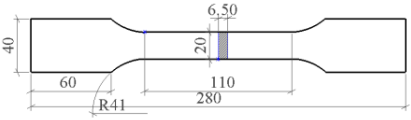

(d) Specimen design for throat

Fig. 15 Specimens for material tensile test

Table 1
Results of material tests

Component	Thickness (mm)	E (10^5 MPa)	f_y (MPa)	f_v (MPa)	f_u (MPa)	f_y/f_u
Throat	6	2.07	370		470	0.78
Hub	6.5	2.05	335	175	464	0.72
Flange	9	2.04	372		560	0.66
Web	6.5	2.07	370		550	0.67

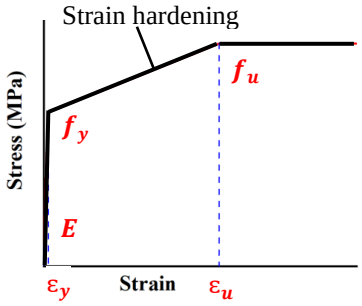

Fig. 16 Material model for components of novel steel dovetail joint

4. Test results and discussion

In this study, the mechanical performance and deformation mechanisms of the two main components of a novel steel dovetail joint system, including the throat and hub, are investigated. Four joint specimens for the two types of interlocks were tested under axial tensile loads. The test program in this study consists of two scenarios: tests of interlock type-I (NDJ) specimens and those of interlock type-II (NDJG) specimens.

4.1. Test results for NDJ specimens

Axial tensile tests were performed on two specimens (NDJ-1 and NDJ-2). The bearing capacity and failure mode were investigated and discussed. At the beginning of the test, a small preload was applied to the specimens to reduce the gap between the beam-inserted end and the keyway of the hub. Thereafter, the working loads were applied through displacement control in the test machine. As the loading increased continuously, the beam end slid slightly, pushing the edges of the keyway in the *Z*-direction (Fig. 17 (a) and (b)). As the loading was continuously applied, the beam-inserted ends (tails) continued to move out, and the hub ring started to expand in the direction of the load (Fig. 17 (c) and (d)). The load–displacement curves of the test, presented in Fig. 18 (a), depict the stiffness and axial tensile bearing capacity of the novel steel dovetail joint.

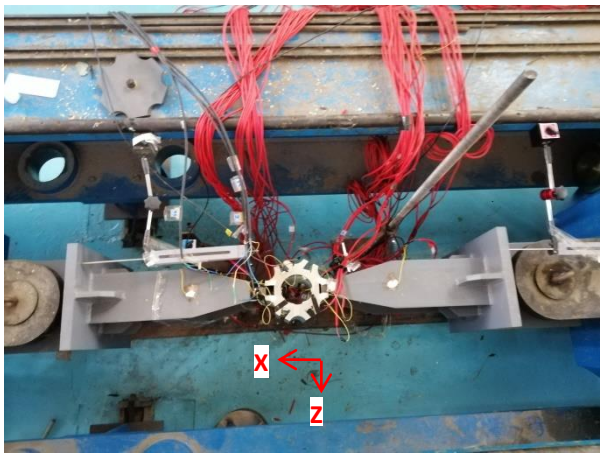

(a) Failure mode of NDJs during the tensile test

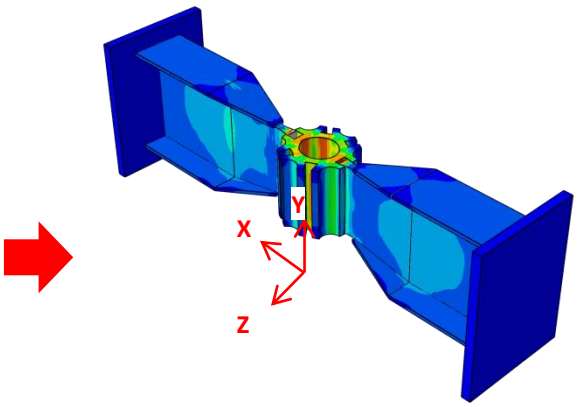

(b) Failure mode of NDJs during the FE analysis

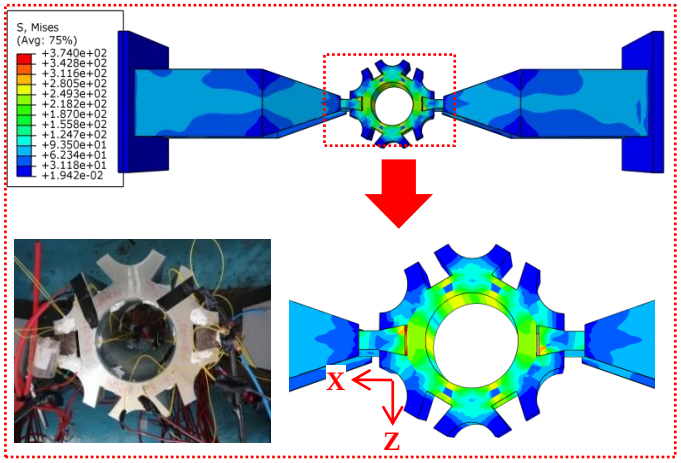

(c) First stage of the failure mode and stress distribution of the NDJs

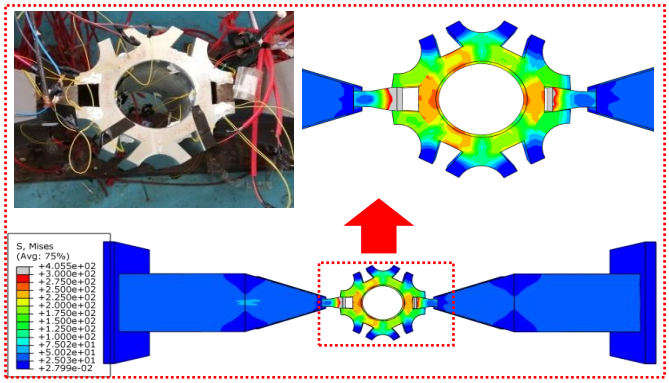

(d) First stage of the failure mode and stress distribution of the NDJs

Fig. 17 Failure modes and stress distributions of NDJs under tensile test and FE analysis

Therefore, it can be seen that the interlock type-I specimens illustrated three load-bearing capacities, including the elastic (N_E^T), yield (N_P^T), and ultimate (N_U^T) capacities; the three capacities for NDJ-1 were 76, 226, and 288 kN, respectively, and 55, 229, and 282.4 kN for NDJ-2. The strain exceeded the yield strain at the measuring points S31, S32, and S39 (in Fig. 18 (b)) and S33, S37, and S38 (in Fig. 18 (c)) of the hub. One side of the interlock component reached the yield capacity in the early loading stage. Therefore, the beam end on this side continued moving out whereas the interlock on the other side stopped moving out. Thus, the hub expanded more on one side than on the other (Fig. 17 (d)). A look at the load–strain curves at the beam measuring points (Fig. 18 (d), (e), and (f)) indicated no deformation in the H-shaped beams of NDJ-1 and NDJ-2 during loading.

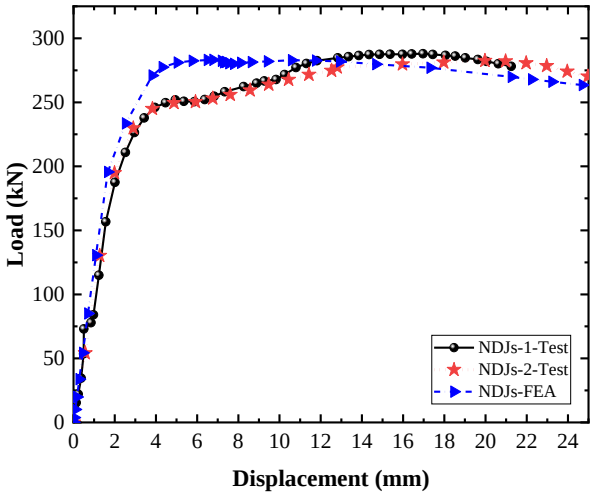

(a) Load–displacement curves

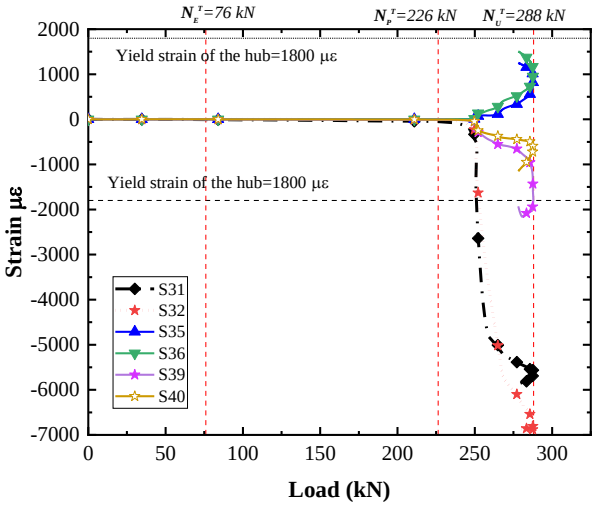

(b)Strain–load curves for the hub

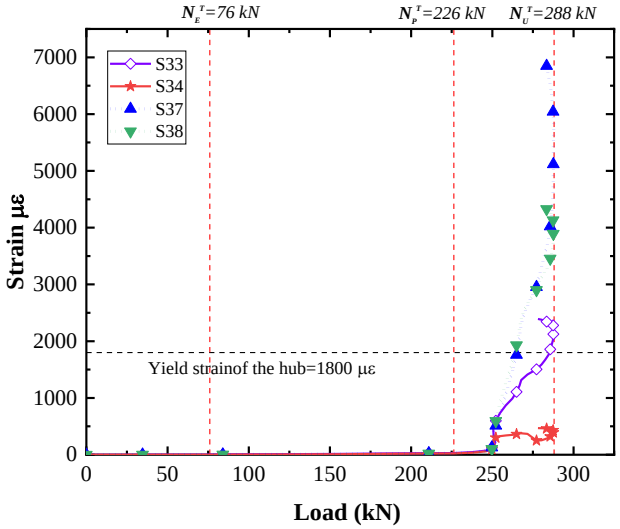

(c) Strain–load curves for the hub

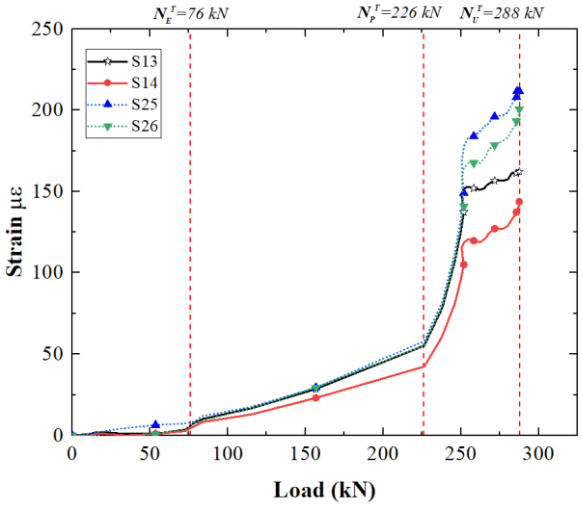

(d) Strain–load curves for the H-shaped beam

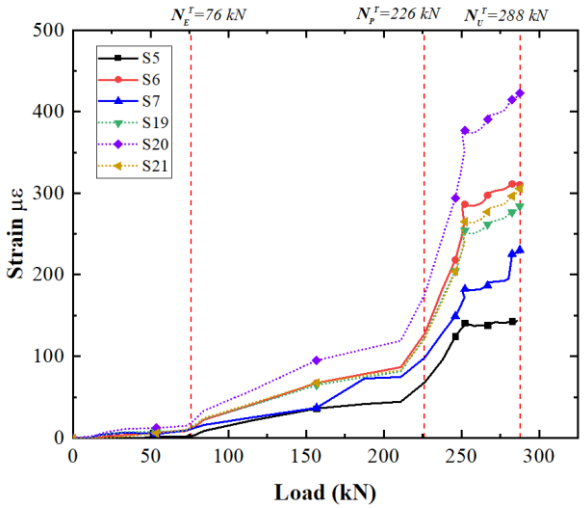

(e) Strain–load curves for the H-shaped beam

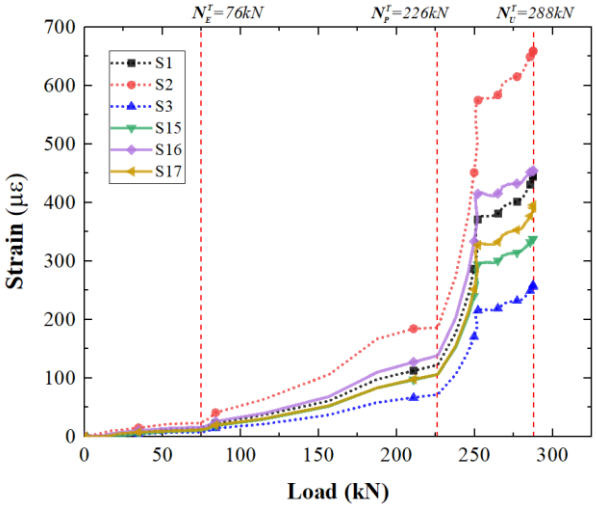

(f) Strain–load curves for the H-shaped beam

Fig. 18 Load–displacement and strain–load curves for the specimens NDJ-1 and NDJ-2

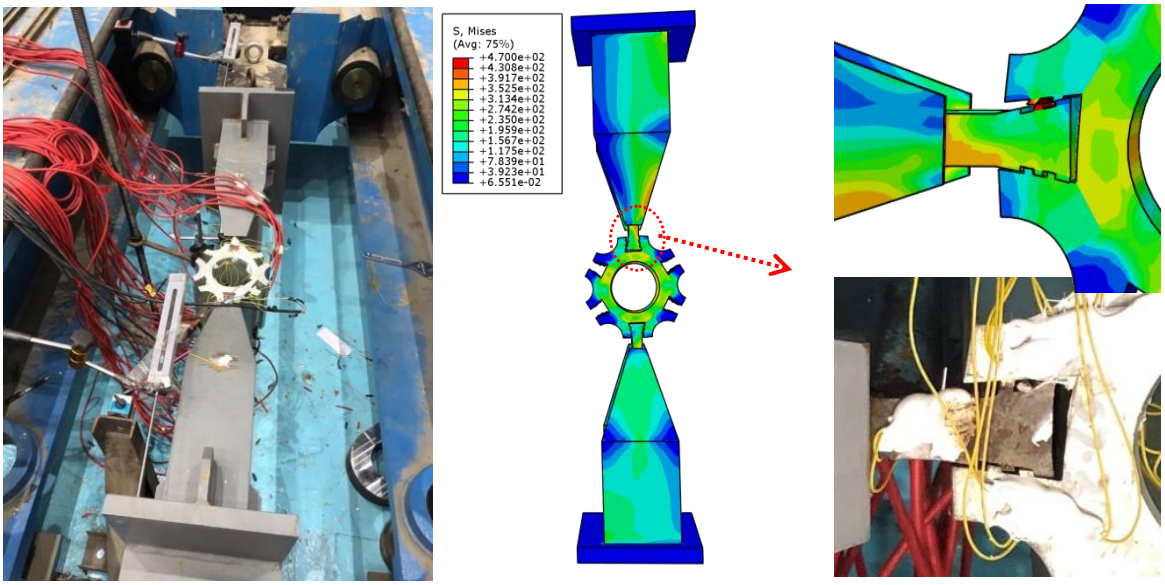

(a) Failure modes of NDJGs during tensile test and FE analysis

(b) First stage of the failure mode and stress distribution

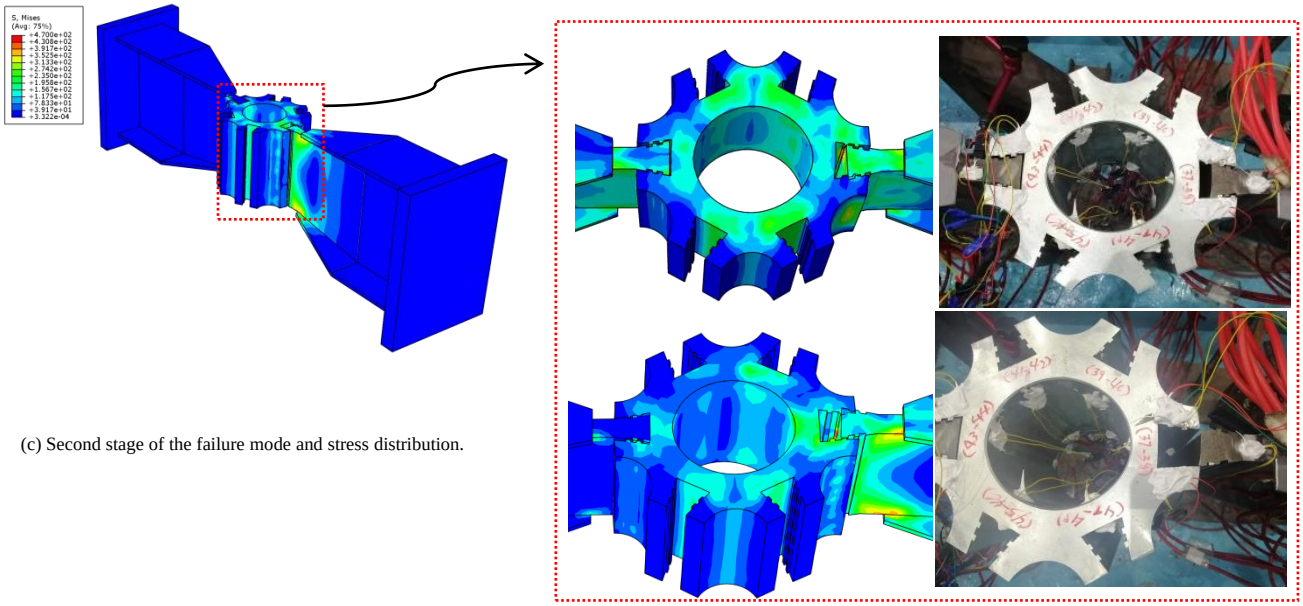

(c) Second stage of the failure mode and stress distribution.

Fig. 19 Failure modes and stress distributions of NDJGs under axial tensile load

4.2. Test results for NDJG specimens

The interlock type-II novel steel dovetail joint specimens (NDJG-1 and NDJG-2) were designed with teeth patterns to increase their bearing capacity and stiffness under axial tensile load. The specimen installation, boundary conditions, and loading process were the same as those described for the interlock type-I specimens in Section 4.1. A preload was applied to set the specimens in the correct loading position and create tightness between the teeth pattern of the interlock component. Thereafter, the working loads were applied by adopting displacement control in the test machine (Fig. 19 (a)). As the loading process continued, the teeth pattern at the beam-inserted end interacted with that in the hub keyway, and the load began to increase. The failure mechanism of the NDJGs was different from that of the NDJs: the latter rely on the friction between the hub keyway and the beam end surfaces to bear the load, whereas the former rely on the friction between the hub keyway and the beam-inserted end as well as on the teeth pattern shear strength. Therefore, shear deformation occurred in the teeth pattern after it reached the material yield capacity (Fig. 19 (b) and (c)).

The elastic (N_E^T), yield (N_P^T), and plastic (N_U^T) capacities for NDJG-1 were 131, 597, and 707 kN, respectively, and 115, 542, and 656 kN for NDJG-2 (Fig. 20 (a)). Specimens with a teeth pattern demonstrated yield and ultimate bearing capacities higher than those without a teeth pattern in the first scenario, where the yield and ultimate tensile bearing capacities of the NDJGs are equal to 2.6 and 2.5 times those of the NDJs. According to the strain results at the measuring points, the neck and teeth pattern of the beam end yielded first, when the strain in the strain gauges S13 and S14 reached the yield capacity (Fig. 20 (b)), whereas the hub had a slide that expanded in the load direction. The interlock teeth pattern on one side reached the yield strength and deformed before that on the other side. Thus, it got cut off and fell down. At that moment, considerable sounds were heard, and the load curves indicate a downward trend when the strain at the measuring points S33, S34, S35, S36, S37, S38, S41, and S42 reached the yield capacity. Further, the hub expanded to increase the space between the edges of the hub keyway (Fig. 20 (c) and (d)). The strains in the beams of NDJG-1 and NDJG-2 were higher than those in the NDJs, particularly around the H-shaped beam with the throat welding area (Fig. 20 (e) and (f)).

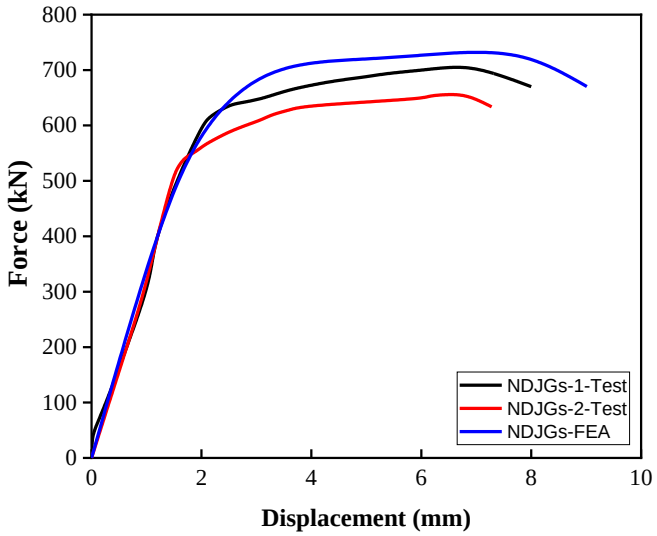

(a) Load–displacement curves

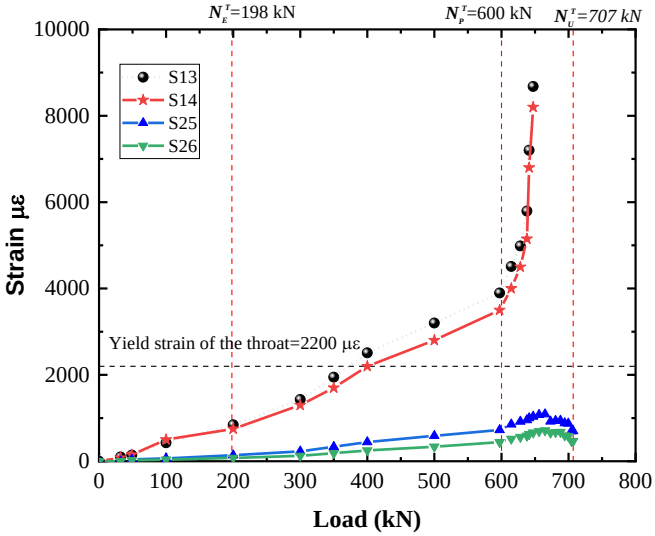

(b) Strain–load curves for the beam

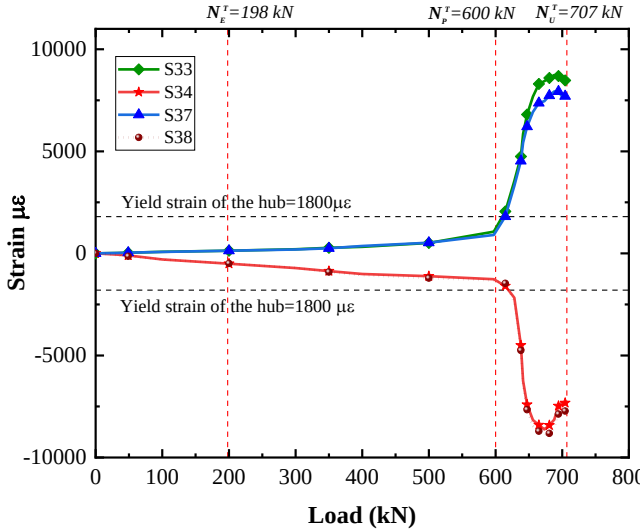

(c) Strain–load curves for the hub ring internal

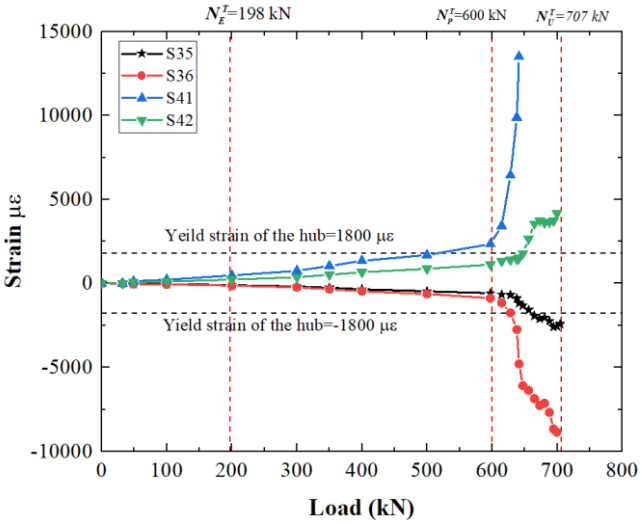

(d) Strain–load curves for the hub ring internal

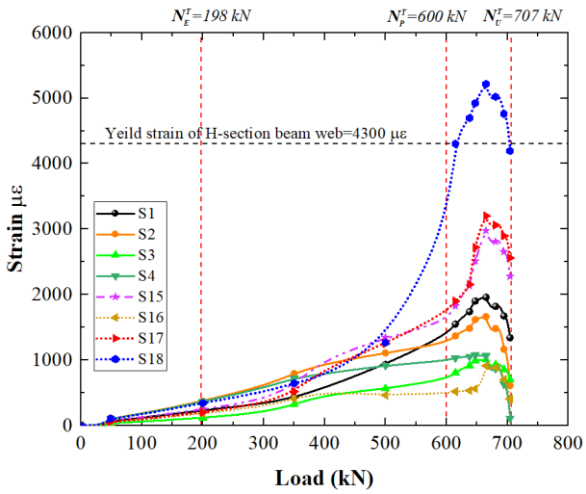

(e) Strain–load curves for the H-shaped beam

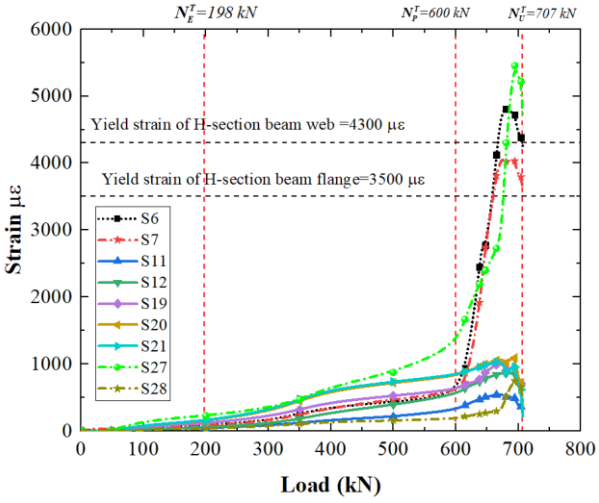

(f) Strain–load curves for the H-shaped beam flanges and welding area

Fig. 20 Load-displacement and strain load curves for specimens NDJG-1 and NDJG-2

5. FE modelling

Based on a dynamic explicit analysis step, full FE models for the NDJs and NDJGs were established using Abaqus software. Because the cover plates, bolts, nuts, and small washers do not affect the tensile bearing capacity of the joints, only hub, throat, and H-section beams were considered in the FE analysis. In the FE analysis, the tensile load was applied to one end of the joint, whereas the other end was fixed. To simplify the FE models, two reference points R1 and R2 were created at the ends of each beam to replace the loading plates in the tests. Based on the test specimen design, a tie contact was adopted

in the Abaqus software to simulate the weld connection in the tested specimens (Figs 21 (a) and Fig. 22 (a)).

5.1. Establishment of FE models

The Solidworks software was used to draw and establish the components of the specimens, including the hubs, throats, and H-shaped beams. All the components of the FE models with interlock type I (NDJ-FE) and interlock type II (NDJG-FE) were imported to Abaqus as Parasolid files for assembly and processing. The material properties for the FE model components are defined according to the material test results presented in Table 1. Before running the analysis, the components were partitioned and meshed with the Hex C3D8R element of all the components (Fig. 23 (a) and (b)). Subsequently, to simulate the boundary conditions in the test, two reference points were defined, and coupling contacts were created between the reference points and the beam ends. Thereafter, contact pair interactions developed in the interlock between the hub and beam-inserted ends. The interactions of NDJ-FE and NDJG-FE were different under tensile loads, where the interaction of surface 2 was suppressed in the interlock system of NDJ-FE, whereas surfaces 1 and 3 were activated. In contrast, the contacts of surfaces 1, 3, and 5 were suppressed, whereas the interactions of surfaces 2 and 4 were activated in the interlock system of NDJG-FE (Figs 21 (b) and 22 (b)).

5.2. Load and boundary conditions

The load and boundary conditions for the FE models of the novel steel dovetail joint were defined based on the boundary conditions (BCs) specified in the test. However, only two BCs were defined for R1 and R2 (Figs 21 and 22). The axial tensile load was applied to R1 as a displacement (U1 = 100 in the *X*-direction), whereas U2 = U3 = UR1 = UR2 = UR3 = 0. In contrast, R2 was considered as a fixed end to allow the joint to move only in the *X*-direction (Fig. 24 (a) and (b)).

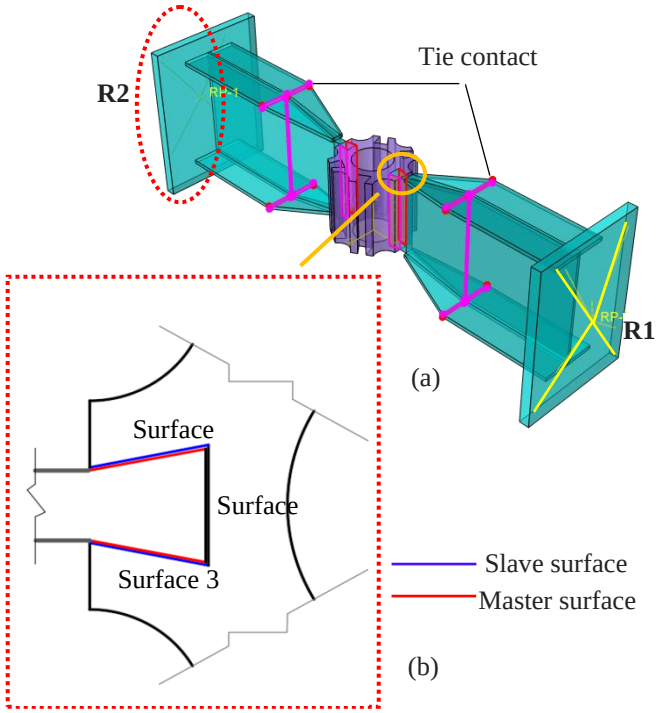

Fig. 21 Interaction details for NDJs: (a) Surface-to-surface, tie, and coupling contacts, (b) interactions in interlock type I

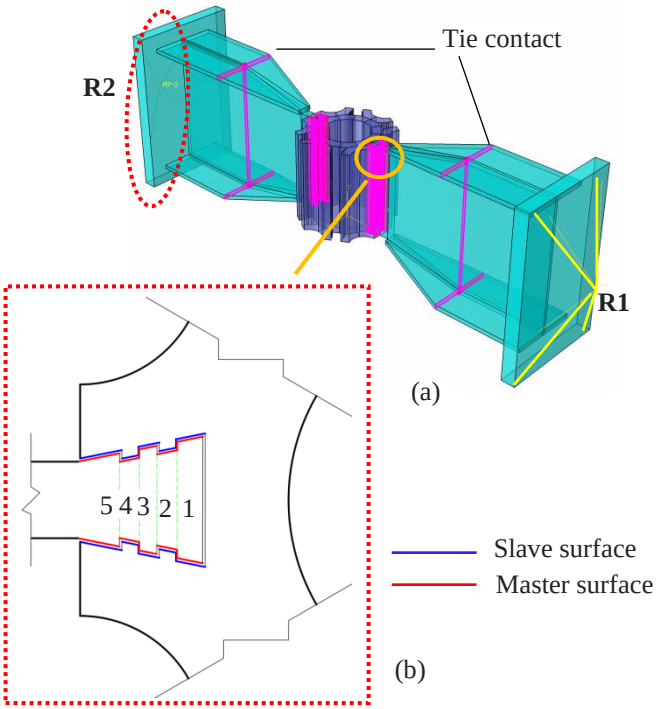

Fig. 22 Interaction details for NDJGs: (a) Surface-to-surface, tie, and coupling contacts, (b) interactions in interlock type II.

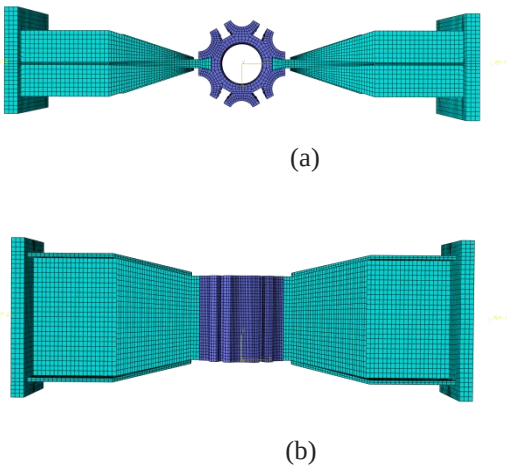

Fig. 23 Mesh for FE models: (a) Top view, (b) side view

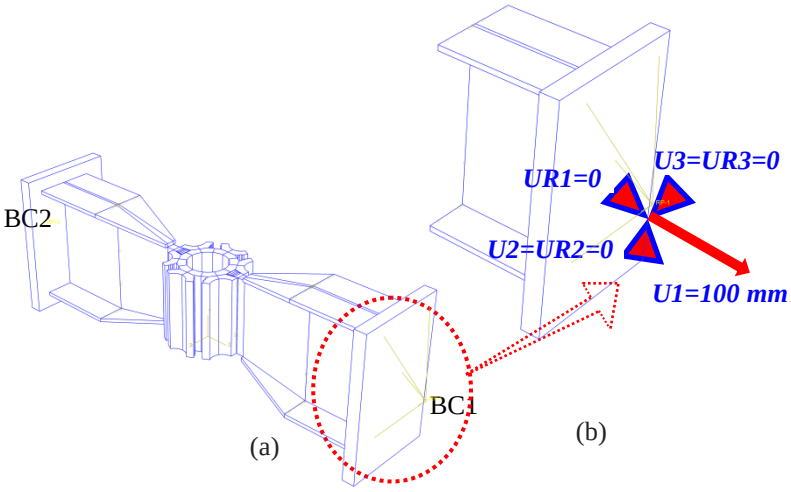

Fig. 24 Load and boundary conditions of FE models: (a) BC1 and BC2, (b) defined load

5.3. FE analysis—results and discussions

The FE models for novel steel dovetail joints without (interlock type I) and with (interlock type II) teeth patterns were analysed to verify the test results of this study. The failure modes and stress distributions of the models were compared with those obtained in the test. The FE model yielded the same stress distribution and failure mechanism (Fig. 17). Moreover, the yield capacity (233 kN) and ultimate tensile bearing capacity (282 kN) obtained using the NDJ-FE were compared with the test results (Fig. 18 (a)); the capacities were very close to the experimental results. In contrast, the

NDJG-FE yielded the same stress distributions and failure modes of the specimens as in the test (Fig. 19). Comparing the tensile capacity results of the FE analysis with the test results (Fig. 20 (a)), the yield capacity for NDJG-FE was 600 kN, which was the same as the yield capacity of NDJG-1 and 1.1 times the yield capacity of NDJG-2. Further, the ultimate capacity for the same model was 733 kN, which is equal to 1.03 times that of NDJG-1 and 1.11 times that of NDJG-2.

The results of the tests and numerical analyses for all the joints are summarised in Fig. 25 and Table 2. It is worth noting that the results of the FE analysis matched well with the test results, with high validity and efficiency.

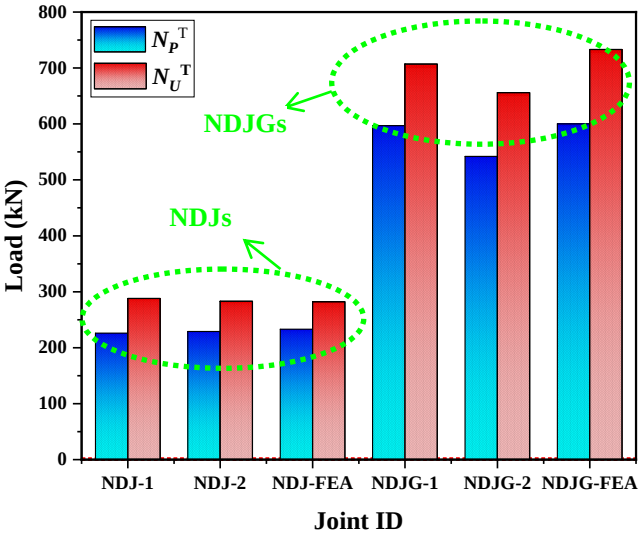

Fig. 25 Comparison of yield and ultimate bearing capacity for NDJs and NDJGs obtained in the test and FE analysis

Table 2
Comparison of yield and ultimate bearing capacities for NDJs and NDJGs obtained in the test and FE analysis

Joint ID	N_P^T times	N_U^T times
NDJG-1/NDJ-1	2.64	2.45
NDJG-1/NDJ-2	2.6	2.5
NDJG-1/NDJG-2	1.06	1.07
NDJG-2/NDJ-1	2.4	2.3
NDJG-2/NDJ-2	2.36	2.33
NDJ-1/NDJ-FEA	0.97	1.02
NDJ-2/NDJ-FEA	0.98	1
NDJG-1/NDJG-FEA	1.0	0.96
NDJG-1/NDJG-FEA	0.9	0.9
NDJG-FEA /NDJ-FEA	2.57	2.6

6. Theoretical analysis for novel steel dovetail joint

Based on the results of the test and FE analysis for the two types of novel steel dovetail joints under axial tensile load, one main failure occurred in NDJ-1 and NDJ-2 when the hub expanded and the beam end was pulled out. In contrast, NDJG-1 and NDJG-2 exhibited the same failure modes noticed in the NDJs accompanied by shear deformation in the interlock teeth. Therefore, theoretically relevant equations of yield and ultimate tensile bearing capacities of the NDJs and NDJGs were derived for the components, considering the design parameters (Figs 26 and 27).

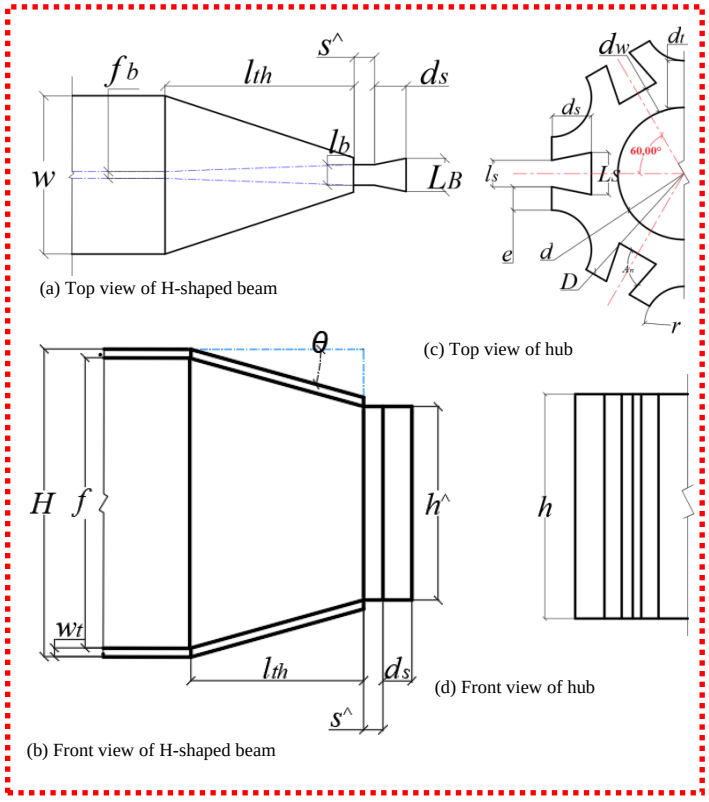

Fig. 26 Design parameters for interlock type-I joints (NDJs)

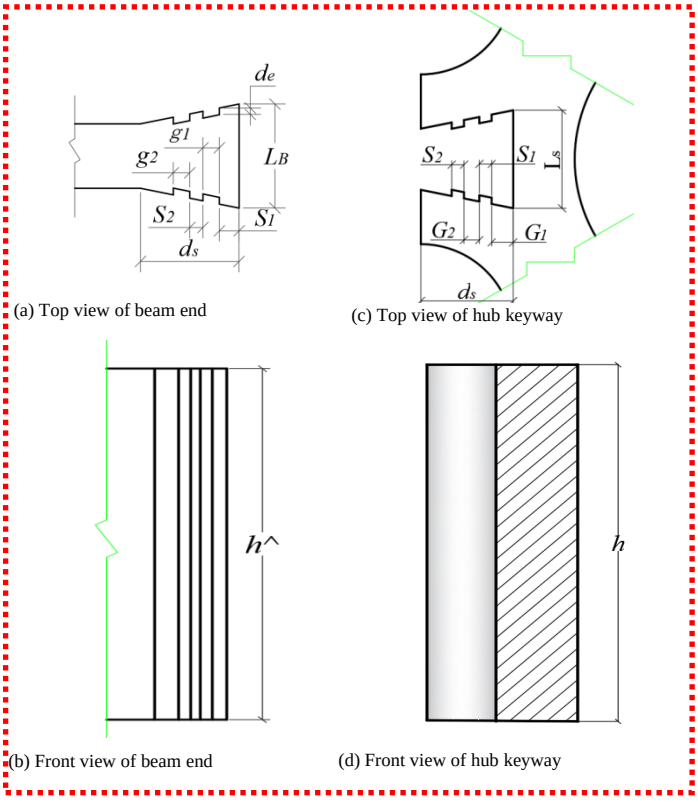

Fig. 27 Design parameters for interlock type-II joints (NDJGs)

6.1. Theoretical analysis of NDJs

Because the shapes of the hub and beam of the novel steel dovetail joint are special, the ring thickness d_w is designed to be the same or larger than the width of the beam neck l_b. Consequently, the following assumptions were adopted to derive the equations for the tensile bearing capacity:

1. The failures in the two edges of the hub keyway occurred simultaneously and had the same magnitude.
2. Based on the results of the test and FE analysis, the failure of the NDJs under tensile load occurred at the hub ring and edges of the hub keyway, where the hub ring is thicker than the neck width ($d_w \geq l_b$). Therefore,

$$T_{\text{neck}}^{Y} = 0.9\, A_{\text{neck}}\, f_y \quad (1)$$

where

$$A_{\text{neck}} = l_b\ h^{\wedge} \quad (2)$$

and $T_{\text{neck}}^{U} = 0.9\, A_{\text{neck}}\, f_u$

where T_{neck}^{Y} and T_{neck}^{U} indicate the tensile yield and ultimate capacities for the beam neck, A_{neck} is the effective area of the beam neck, l_b denotes the width of the beam neck, $h^{\wedge}$is the neck height, and f_y and f_u are the material yield and ultimate strength, respectively.

3. The deformed section area of the edges of the hub keyway was assumed to be equal to the thickness of the hub ring. Therefore, the tensile yield-bearing capacity of hub type I, where $d_{\text{m}} = d_{\text{w}} = 0.2d = 0.1D \geq l_b$, can be expressed as follows:

$$N_{P,\text{th}}^{T} = \frac{0.11\ d_m\ d_w\ h^{\wedge}\ f_v\ d_s}{D} \quad (3)$$

and the ultimate tensile bearing capacity can be expressed as follows:

$$N_{U,\text{th}}^{T} = \frac{1.5\ d_m\ d_w\ h^{\wedge}\ f_u}{D} \quad (4)$$

6.2. Theoretical analysis of NDJGs

The NDJGs rely on the hub ring, edges of the hub keyway, and teeth patterns to bear the tensile load. The tensile bearing capacity of NDGs is 2.5 times higher than that of the NDJs. Based on the results of the test and numerical analysis, the NDJG-type combined hub ring, hub keyway edge failures, and teeth pattern shear failures under axial tensile load. However, the tensile yield capacity of the NDJGs can be expressed as follows:

$$N_{P,\text{th}}^{T} = \left(\frac{\left(1.4\ D\ (l_n)^2\right)+\left(0.11\ d_m\ d_w\ (d_s)^2\right)}{D\ d_s}\right) h^{\wedge}\ f_v \quad (5)$$

Moreover, the ultimate tensile bearing capacity can be expressed as follows:

$$N_{U,\text{th}}^{T} = \left(\frac{\left(0.63\ D\ (l_n)^2\right)+\left(1.5\ d_m\ d_w\ d_s\ \right)}{D\ d_s}\right) h^{\wedge}\ f_u \quad (6)$$

where l_n is the total width of the teeth:

$$l_n = S_1 + S_2 + \ldots + S_n$$

7. Validations of test, FE analysis, and theoretical analysis

This section presents the calculations and comparisons of the results of the test and the numerical and theoretical analyses of the novel steel dovetail joint, as summarised in Table 3. The results of the analyses of the three approaches adopted in this study were validated by calculating the mean values of the ratios of the theoretical to test, theoretical to numerical, and test to numerical results for the NDJs and NDJGs. Based on the results of the comparison of the three methods of analysis, the standard deviation (Std v) was also calculated; its maximum value was 0.056. The tensile yield and ultimate bearing capacities of the NDJs and NDJGs obtained by adopting the three methods of analysis matched well with each other and indicated very high efficiency and validity.

Table 3
Comparison of the results of the test, FE analysis, and theoretical analysis for tensile bearing capacity

Item	$N_{P,t}^{T}$	$N_{P,n}^{T}$	$N_{P,\text{th}}^{T}$	$N_{P,\text{th}}^{T}$ /$N_{P,t}^{T}$	$N_{P,\text{th}}^{T}$ /$N_{P,n}^{T}$	$N_{P,t}^{T}$/ $N_{P,n}^{T}$	$N_{U,t}^{T}$	$N_{U,n}^{T}$	$N_{U,\text{th}}^{T}$	$N_{U,\text{th}}^{T}$ /$N_{U,t}^{T}$	$N_{U,\text{th}}^{T}$ /$N_{U,n}^{T}$	$N_{U,t}^{T}$/ $N_{U,n}^{T}$
NDJ-1	226	233	231	1.02	0.99	0.97	288	282	282	0.98	1	1.0
NDJ-2	229	233	231	1.01	0.99	0.98	283	282	282	0.99	1	1.003
NDJG-1	597	600	598	1.0	0.99	0.99	707	733	726	1.02	0.99	0.96
NDJG-2	542	600	598	1.1	0.99	0.90	656	733	726	1.10	0.99	0.89
Average				1.03	0.99	0.96				1.03	0.99	0.97
Std v				0.047	0.003	0.041				0.056	0.005	0.056

8. Conclusions

The single-layer lattice steel structure system is one of the most developed and young systems in the field of steel structures. Various types of joints with various types of structural element sections and materials have been designed and studied to fulfil the structural requirements. In this study, interlock type-I () and interlock type-II () novel steel dovetail joints (NDJs and NDJGs, respectively) were proposed and tested. Based on the results of the analysis, the following conclusions were drawn:

1. The novel steel dovetail joint design concept, design method, FE modelling method, and test program have been proposed and discussed using an H-shaped beam to gather and present detailed information on the new joint system.
2. The test and FE analyses were carried out on novel steel dovetail joints with different interlock-type systems. The two types presented different tensile bearing capacities: the tensile yield and ultimate bearing capacities of the interlock type-II specimens were 2.4–2.64 times those of the interlock type-I specimens.
3. Based on the results of the test and FE analysis, the NDJs and NDJGs presented different deformation modes based on their respective failure mechanisms: The NDJs rely on the interlock system and hub ring to bear the load. Therefore, a major failure occurred in the hub ring. In contrast, the NDJGs rely on the interlock system, hub ring, and teeth patterns to bear the load. Therefore, the NDJGs combined two failure modes: the hub ring expanding failure and teeth pattern shear failure.
4. The related equations for the tensile yield and ultimate bearing capacities of the NDJs and NDJGs were proposed and calculated. As experimental, numerical, and theoretical approaches were adopted to investigate the mechanical performance and failure modes of the novel steel dovetail joints, the theoretical and numerical results for the two groups verified the experimental results. All the results obtained using the three approaches in this study matched very well and indicated high analysis validity and efficiency.

Acknowledgements

This study was financially supported by the Natural Science Foundation of Hebei Province (Grant No. E2021402006).

List of symbols

NDJs	Novel steel dovetail joint without teeth pattern (interlock type I)	$s^{\wedge}$	Neck's length (mm)
		t_h	Length of H-shaped beam end (mm)
NDJGs	Novel steel dovetail joint with teeth pattern (interlock type II)	θ	Slope angle of throat
Design NDJ symbols		$S_1,\ S_2$	Teeth width (mm)
D	External diameter of hub (mm)	G_1, G_2	Groove in hub keyway (mm)

d	Internal diameter of hub (mm)	g_1, g_2	Groove in beam end (mm)
d_s	Keyway length of hub (mm)	d_e	Groove depth (mm)
d_w	Thickness of hub ring (mm)	***Theoretical analysis symbols***	
d_t	Maximum thickness of hub (mm)	l_n	Total width of teeth pattern (mm)
r	Diameter of removed area (mm)	$T^Y_{\mathbf{neck}}$	Beam neck tensile yield-bearing capacity
L_s	Maximum width of hub keyway (mm)	$A_{\mathbf{neck}}$	Section area of beam neck
l_s	Minimum width of hub keyway (mm)	$T^U_{\mathbf{neck}}$	Beam neck ultimate tensile bearing capacity
h	Hub height (mm)	$N^T_{P,\mathrm{th}}$	Yield capacity in equations
e	Width of edge of hub keyway (mm)	$N^T_{P,t}$	Yield bearing capacity in test
H	Height of H-shaped beam (mm)	$N^T_{P,n}$	Yield bearing capacity of FE analysis
$\mathrm{h}^{\wedge}$	Height of H-shaped beam end (mm)	$N^T_{U,t}$	Ultimate bearing capacity in test
L_B	Maximum width of beam end (mm)	$N^T_{U,n}$	Ultimate bearing capacity in FE analysis
l_b	Minimum width of beam end (mm)	$N^T_{U,\mathrm{th}}$	Ultimate bearing capacity in equations
f_b	Thickness of H-shaped beam web (mm)	E	Elastic modulus
w_t	Thickness of H-shaped beam flange (mm)	f_y	Material yield strength (kN)
w	Flange width of H-shaped beam (mm)	f_u	Material ultimate strength (kN)
f	Web height of H-shaped beam (mm)	f_v	Material shear strength (kN)
l_{th}	Length of throat (mm)	ε_y	Material yield strain

References

[1] R. qiang Feng, X. Wang, Y. Chen, and Q. Cai, "Static performance of double-ring joints for freeform single-layer grid shells subjected to a bending moment and shear force," Thin-Walled Struct., vol. 131, no. December 2017, pp. 135–150, 2018, doi: 10.1016/j.tws.2018.06.038.

[2] Q. Han, C. Wang, Y. Xu, X. Zhang, and Y. Liu, "Mechanical performance of AH joints and influence on the stability behaviour of single-layer cylindrical shells," Thin-Walled Struct., vol. 146, no. June 2019, p. 106459, 2020, doi: 10.1016/j.tws.2019.106459.

[3] Q. Han, Y. Liu, J. Zhang, and Y. Xu, "Mechanical behaviors of the Assembled Hub (AH) joints subjected to bending moment," J. Constr. Steel Res., vol. 138, pp. 806–822, 2017, doi: 10.1016/j.jcsr.2017.08.026.

[4] Y. Y. Ma, H. H. Ma, F. Fan, and Z. W. Yu, "Experimental and theoretical analysis on static behavior of bolt-column joint under in-plane direction bending in single-layer reticulate shells," Thin-Walled Struct., vol. 135, no. November 2018, pp. 472–485, 2019, doi: 10.1016/j.tws.2018.11.009.

[5] H. Liu, H. Chen, and Z. Chen, "Residual behaviour of welded hollow spherical joints under corrosion and de-rusting," J. Constr. Steel Res., vol. 167, p. 105977, 2020, doi: 10.1016/j.jcsr.2020.105977.

[6] J. Lu, H. Liu, and Z. Chen, "Behavior of welded hollow spherical joints after exposure to ISO-834 standard fire," J. Constr. Steel Res., vol. 140, pp. 108–124, 2018, doi: 10.1016/j.jcsr.2017.10.026.

[7] H. Nassiraei, M. A. Lotfollahi-Yaghin, H. Ahmadi, and L. Zhu, "Static strength of doubler plate reinforced tubular T/Y-joints under in-plane bending load," J. Constr. Steel Res., vol. 136, no. April, pp. 49–64, 2017, doi: 10.1016/j.jcsr.2017.05.009.

[8] S. Stephan, K. Knebel, and J. Sanchez-Alvarez, "Reticulated Structures On Free-Form Surfaces," Stahlbau, vol. 73, no. April, pp. 562–572, 2004.

[9] Ma. H, Fan. F, & Shen. S, "NUMERICAL PARAMETRIC INVESTIGATION OF SINGLE-LAYER LATTICED DOMES WITH SEMI-RIGID JOINTS, " J. Journal-International Association for Shell and Spatial Structures, 49, 99-110.

[10] A. L. Zhang, G. H. Shangguan, Y. X. Zhang, Q. B. Wang, and W. C. Cai, "Experimental study of resilient prefabricated steel frame with all-bolted beam-to-column connections," Adv. Steel Constr., vol. 16, no. 3, pp. 255–271, 2020, doi: 10.18057/IJASC.2020.16.3.7.

[11] H. W. Ma, H. Zheng, W. Zhang, and Z. Z. Tang, "Experimental and numerical study of mechanical properties for the double-ribbed reinforced beam-column connection," Adv. Steel Constr., vol. 16, no. 4, pp. 297–309, 2020, doi: 10.18057/IJASC.2020.16.4.2.

[12] H. Ma, L. Yu, F. Fan, and Z. Yu, "Mechanical performance of an improved semi-rigid joint system under bending and axial forces for aluminum single-layer reticulated shells," Thin-Walled Struct., vol. 142, no. May, pp. 322–339, 2019, doi: 10.1016/j.tws.2019.05.003.

[13] H. Ma, F. Fan, G. Chen, Z. Cao, and S. Shen, "Numerical analyses of semi-rigid joints subjected to bending with and without axial force," J. Constr. Steel Res., vol. 90, pp. 13–28, 2013, doi: 10.1016/j.jcsr.2013.07.017.

[14] M. Ahmadizadeh and S. Maalek, "An investigation of the effects of socket joint flexibility in space structures," J. Constr. Steel Res., vol. 102, pp. 72–81, 2014, doi: 10.1016/j.jcsr.2014.07.001.

[15] Zhao. C, Liu. W, Zhao. H, Elastic Plastic Analysis and Experimental Research on New Joint of Reticulated Shells ," J. Journal of Southeast University, Vol.28 No.2 Mar .1998. [in Chinese]

[16] W. T. Qiao, R. J. Zhu, D. Wang, J. Li, and J. W. Yuan, "Study on moment-rotation relationship of steel sleeve beam-column joint with interference fit," Adv. Steel Constr., vol. 16, no. 4, pp. 337–345, 2020, doi: 10.18057/IJASC.2020.16.4.6.

[17] S. Yan, K. J. R. Rasmussen, L. L. Jiang, C. Zhu, and H. Zhang, "Experimental evaluation of the full-range behaviour of steel beam-to-column connections," Adv. Steel Constr., vol. 16, no. 1, pp. 77–84, 2020, doi: 10.18057/IJASC.2020.16.1.9.

[18] Z. Xiong, X. Guo, Y. Luo, and H. Xu, "Numerical analysis of aluminium alloy gusset joints subjected to bending moment and axial force," Eng. Struct., vol. 152, pp. 1–13, 2017, doi: 10.1016/j.engstruct.2017.09.005.

[19] Q. Han, Y. Liu, Y. Xu, and Z. Li, "Mechanical behaviours of assembled hub joints subjected to axial loads," J. Constr. Steel Res., vol. 153, pp. 667–685, 2019, doi: 10.1016/j.jcsr.2018.11.007.

[20] H. Ma, Y. Ma, Z. Yu, and F. Fan, "Experimental and numerical research on gear-bolt joint for free-form grid spatial structures," Eng. Struct., vol. 148, pp. 522–540, 2017, doi: 10.1016/j.engstruct.2017.06.076.

[21] G. Oyéniran ADEOTI, F. Fan, M. A. Huihuan, and S. Shen, "Investigation of aluminium bolted joint (HBJ) system behavior," Thin-Walled Struct., vol. 144, no. June 2016, p. 106100, 2019, doi: 10.1016/j.tws.2019.03.059.

[22] F. Fan, H. Ma, G. Chen, and S. Shen, "Experimental study of semi-rigid joint systems subjected to bending with and without axial force," J. Constr. Steel Res., vol. 68, no. 1, pp. 126–137, 2012, doi: 10.1016/j.jcsr.2011.07.020.

[23] H. Ma, S. Ren, and F. Fan, "Experimental and numerical research on a new semi-rigid joint for single-layer reticulated structures," Eng. Struct., vol. 126, pp. 725–738, 2016, doi: 10.1016/j.engstruct.2016.08.028.

[24] K. D. Tsavdaridis, R. Feng, and F. Liu, "Shape Optimization of Assembled Single-Layer Grid Structure with Semi-Rigid Joints," Procedia Manuf., vol. 44, no. 2019, pp. 12–19, 2020, doi: 10.1016/j.promfg.2020.02.199.

[25] Y. Y. Ma, H. H. Ma, S. Ren, and F. Fan, "Hysteretic behavior of a new assemble joint under out-of-plane bending: Experimental and numerical studies," J. Constr. Steel Res., vol. 167, pp. 1–14, 2020, doi: 10.1016/j.jcsr.2020.105959.

[26] S. D. Xue, S. Y. Li, X. Y. Li, and C. Yao, "Behaviour and mathematical model for semi-rigid threaded-sleeve connection," Adv. Steel Constr., vol. 15, no. 2, pp. 123–128, 2019, doi: 10.18057/IJASC.2019.15.2.1.

[27] H. Wang, Q. Wu, H. Qian, K. Han, and F. Fan, "Buckling behavior of a circular steel tube with a bolt–ball joint under installation eccentricity," Eng. Struct., vol. 197, no. July, p. 109407, 2019, doi: 10.1016/j.engstruct.2019.109407.

[28] H. Chen, H. Liu, and Z. Chen, "Compressive strength of corroded special-shaped welded hollow spherical joints based on numerical simulation," Thin-Walled Struct., vol. 149, no. May 2019, p. 106531, 2020, doi: 10.1016/j.tws.2019.106531.

[29] H. Liu, Y. Ding, and Z. Chen, "Static stability behavior of aluminum alloy single-layer spherical latticed shell structure with Temcor joints," Thin-Walled Struct., vol. 120, no. June, pp. 355–365, 2017, doi: 10.1016/j.tws.2017.09.019.

[30] Z. Xiong, X. Guo, Y. Luo, S. Zhu, and Y. Liu, "Experimental and numerical studies on single-layer reticulated shells with aluminium alloy gusset joints," Thin-Walled Struct., vol. 118, no. March, pp. 124–136, 2017, doi: 10.1016/j.tws.2017.05.007.

[31] H. Liu, Y. J. Zhang, L. Wang, Y. Zhao, and Z. H. Chen, "Mechanical performance of welded hollow spherical joints with H-beams after elevated temperatures," Eng. Struct., vol. 222, no. January, p. 111092, 2020, doi: 10.1016/j.engstruct.2020.111092.

[32] X. Li, J. Zhao, G. Ma, and W. Chen, "Experimental study on the seismic performance of a double-span traditional timber frame," Eng. Struct., vol. 98, pp. 141–150, 2015, doi: 10.1016/j.engstruct.2015.04.031.

[33] Q. Xie, L. Zhang, L. Wang, W. Zhou, and T. Zhou, "Lateral performance of traditional Chinese timber frames: Experiments and analytical model," Eng. Struct., vol. 186, no. February, pp. 446–455, 2019, doi: 10.1016/j.engstruct.2019.02.038.

[34] C. Chen, H. Qiu, and Y. Lu, "Flexural behaviour of timber dovetail mortise-tenon joints," Constr. Build. Mater., vol. 112, pp. 366–377, 2016, doi: 10.1016/j.conbuildmat.2016.02.074.

[35] "Chinese Metalic materials-Tensile testing-part 1: Method of test at room temperature". GB/T 228.1-2010.